Journal of Hydraulic Research Vol. 42, No. 1 (2004), pp. 43–54

Hydraulics of stepped chutes: The transition flow

L'hydraulique des chutes en marches d'escalier: L'écoulement de transition

H. CHANSON, *Reader, Fluid Mechanics, Hydraulics and Environmental Engineering, The University of Queensland, Brisbane QLD 4072, Australia. Email: h.chanson@uq.edu.au*

LUKE TOOMBES, *Associate Lecturer, Fluid Mechanics, Department of Civil Engineering, The University of Queensland, Brisbane QLD 4072, Australia*

ABSTRACT
Stepped spillway flows may behave as a succession of free-falling nappes at low flows and as a skimming flow at large discharges. However there is a range of intermediate flow rates characterised by a chaotic flow motion associated with intense splashing: i.e. the transition flow regime. Detailed air–water flow properties in transition flows were measured in two large experimental facilities. The results provide a complete characterisation of the air concentration, velocity and bubble count rate distributions. They highlight some difference between the upper and lower ranges of transition flows in terms of longitudinal free-surface profiles and air concentration distributions. Overall a dominant feature is the very-strong free-surface aeration, well in excess of observed data in smooth-invert and skimming flows.

RÉSUMÉ
Les écoulements sur les déversoirs en marches d'escalier peuvent se comporter comme une succession des nappes en chute libres aux faibles débits et comme un écoulement écumant aux grands débits. De sorte qu'il y a toute une gamme de débits intermédiaires caractérisés par un mouvement chaotique d'écoulement lié à un éclaboussement intense: i.e. le régime d'écoulement de transition. Des propriétés détaillées de l'écoulement du mélange air-eau dans des écoulements de transition ont été mesurées dans deux grands équipements expérimentaux. Les résultats fournissent une caractérisation complète de la concentration d'air, des distributions de vitesse et du taux de bulles. Ils mettent en lumière une certaine différence entre les gammes supérieures et inférieures des écoulements de transition en termes de profils de surface libre et distributions longitudinales de concentration en air. De façon générale un caractère dominant est l'aération très forte de surface libre, bien au-dessus des données observées dans les écoulements lisses inversés et écumants.

Keywords: Stepped spillway; transition flow regime; free-surface aeration; chaotic flow pattern; experimental study.

Introduction

In a stepped chute, low flows behave as a succession of free-falling nappes: i.e. the nappe flow or jet flow regime (e.g. Horner, 1969). For a given step and chute geometry, large flows skim over the pseudo-invert formed by the step edges: i.e. the skimming flow regime. The cavity formed by the steps is filled and strong cavity recirculation is observed beneath the main stream (e.g. Rajaratnam, 1990). The conditions for the transition from nappe to skimming flows were discussed by Chanson (1996) and Chamani and Rajaratnam (1999) who used the term "*onset of skimming flow*". Few researchers discussed specifically the transitory flow conditions between nappe and skimming flow: e.g. Elviro and Mateos (1995). Ohtsu and Yasuda (1997) were the first to define the concept of a "*transition flow*" regime although they did not elaborate on its flow properties. Up to date little information is available on transition flows.

It is the purpose of this study to provide a comprehensive study of transition flows down stepped chutes. Air–water flow measurements were conducted in two large facilities with slopes ranging from 3.4 to 22° and equipped with large step heights. A detailed characterisation of the air–water flow properties is provided.

Experimental configuration

New experiments were conducted at the University of Queensland in two large-size facilities (Table 1). One facility was a 24-m long 0.5-m wide channel made of planed wooden boards. Two stepped inverts were used. The flume 1 consisted of ten 0.143-m high, 2.4-m long horizontal steps while flume 2 had eighteen 0.071-m high, 1.2-m long flat steps. For all experiments, the first drop was located 2.4 m downstream of a smooth nozzle, and the channel invert upstream of the vertical drop was flat and horizontal. Water was supplied by a pump, with a variable-speed electronic controller (Taian^{TM} T-verter K1-420-M3 adjustable frequency AC motor drive), enabling an accurate

Revision received June 12, 2003. Open for discussion till June 30, 2004.

Table 1 Summary of experimental flow configurations.

Ref.	α deg.	h m	q_w m^2/s	Observed flow regime	Remarks
(1)	(2)	(3)	(4)	(5)	(6)
Flume 1	3.4	0.143	0.08–0.140	Nappe & Transition flows	L = 24 m. W = 0.5 m. Supercritical inflow: d_o = 0.03 m. Flat horizontal steps. Experiments CR98.
Flume 1	3.4	0.071	0.08–0.130	Nappe, Transition & Skimming flows	L = 24 m. W = 0.5 m. Supercritical inflow: d_o = 0.03 m. Flat horizontal steps. Experiments EV200a.
Flume 3	21.8	0.10	0.04–0.18	Nappe, Transition & Skimming flows	L = 3.0 m. W = 1 m. Broad-crest with smooth inflow sidewall convergent (4.8 : 1 contraction). Low upstream turbulence. Flat horizontal steps. Experiments EV200b & TC200.
Flume 4	15.9	0.10	0.05–0.26	Nappe, Transition & Skimming flows	L = 4.2 m. W = 1 m. Broad-crest with smooth inflow sidewall convergent (4.8 : 1 contraction). Low upstream turbulence. Flat horizontal steps. Experiments TC201.

Notes: h = step height; L = chute length; W = chute width.

discharge adjustment in a closed-circuit system. The flow rates were measured with a Dall™ tube flowmeter, calibrated on site. The accuracy on the discharge measurement was about 2%.

Another channel was 5-m long, 1-m wide. Waters were supplied from a large feeding basin leading to a sidewall convergent. Two slopes were tested. One geometry consisted of a 0.88-m long broad-crested weir with upstream rounded corner followed by nine identical steps (h = 0.1 m, l = 0.35 m) made of marine ply. The second geometry consisted of a 0.6-m long broad-crested weir followed by nine steps (h = 0.1 m, l = 0.25 m). The stepped chute was 1-m wide with perspex sidewalls, followed by a horizontal concrete-invert canal ending in a dissipation pit. The flow rate was delivered by a pump controlled with an adjustable frequency AC motor drive, enabling an accurate discharge adjustment in a closed-circuit system. The discharge was measured from the upstream head above crest with an accuracy of about 2% (Bos, 1976). Figure 1 illustrates the chute geometry.

Further details on the experimental facilities may be found in Chanson and Toombes (1998, 2001).

Instrumentation and measurement techniques

Clear-water flow depths and velocities were measured with a point gauge and a Prandtl–Pitot tube ($\oslash$ = 3.3 mm) respectively. Air–water flow properties were measured using single-tip and double-tip conductivity probes. For the double-tip probe, the probe sensors ($\oslash$ = 0.025 mm, 7.775 mm spacing between sensors) were aligned in the flow direction. The probes were excited by an air bubble detector (AS25240). The probe signal was scanned at 5 kHz for 60 to 180 s for the single-tip probe and at 20 kHz for 20 to 40 s per sensor for the double-tip probe. The translation of the probes in the direction normal to the channel invert was controlled by a fine adjustment travelling mechanism connected to a Mitutoyo™ digimatic scale unit. The error on the probe position was less than 0.025 mm. The accuracy on the longitudinal position of the probe was estimated as $\Delta x < \pm 0.5$ cm. The accuracy on the transverse position of the probe was less than 1 mm. Flow visualisations were conducted with a digital video-camera Sony™ CCD TRV900 (shutter: 1/4 to 1/10,000 s) and high-speed still photographs.

Experiments were conducted for flow rates ranging from 0.04 to 0.2 m^3/s (Table 1). On the steepest slopes (16° & 22°), air–water measurements were conducted at the step edges and at half-distance between step edges (Fig. 1). The position y of the probes was measured normal to the pseudo-invert formed by the step edges. On the flat slope, measurements were performed at the step edges and at several intermediate locations. The vertical position y of the probes was measured normal to the horizontal step face: i.e. along the true vertical.

Distributions of air concentrations and bubble count rates[1] were recorded in all experimental facilities. Distributions of air-water velocities were performed in the 16 and 22° stepped chutes only.

Similitude and scale effects

The study was conducted based upon a Froude similitude. Both facilities were wide enough to achieve two-dimensional flows and measurements were conducted on the channel centreline. The large size of the two experimental facilities in terms of step heights and flow rates ensures that the experimental results may be extrapolated to prototype with negligible scale effects for geometric scaling ratios less than 10 : 1. For larger prototype to model scaling ratios, some scale effects may take place in terms in flow resistance, free-surface aeration and energy dissipation as demonstrated by BaCaRa (1991), Chanson (1997) and Chanson *et al.* (2000).

Experimental results: (1) Flow patterns

The facilities were designed to operate with flow conditions ranging from nappe to skimming flow regimes, although the focus of the study was on the transition flow regime. For a given chute geometry, low discharges flowed down the chute as a succession of clear, distinct free-falling nappes (i.e. nappe flow regime). For large discharges, the flow skimmed over the pseudo-bottom

[1]also called bubble frequency, defined as the number of bubbles impacting the probe tip per second.

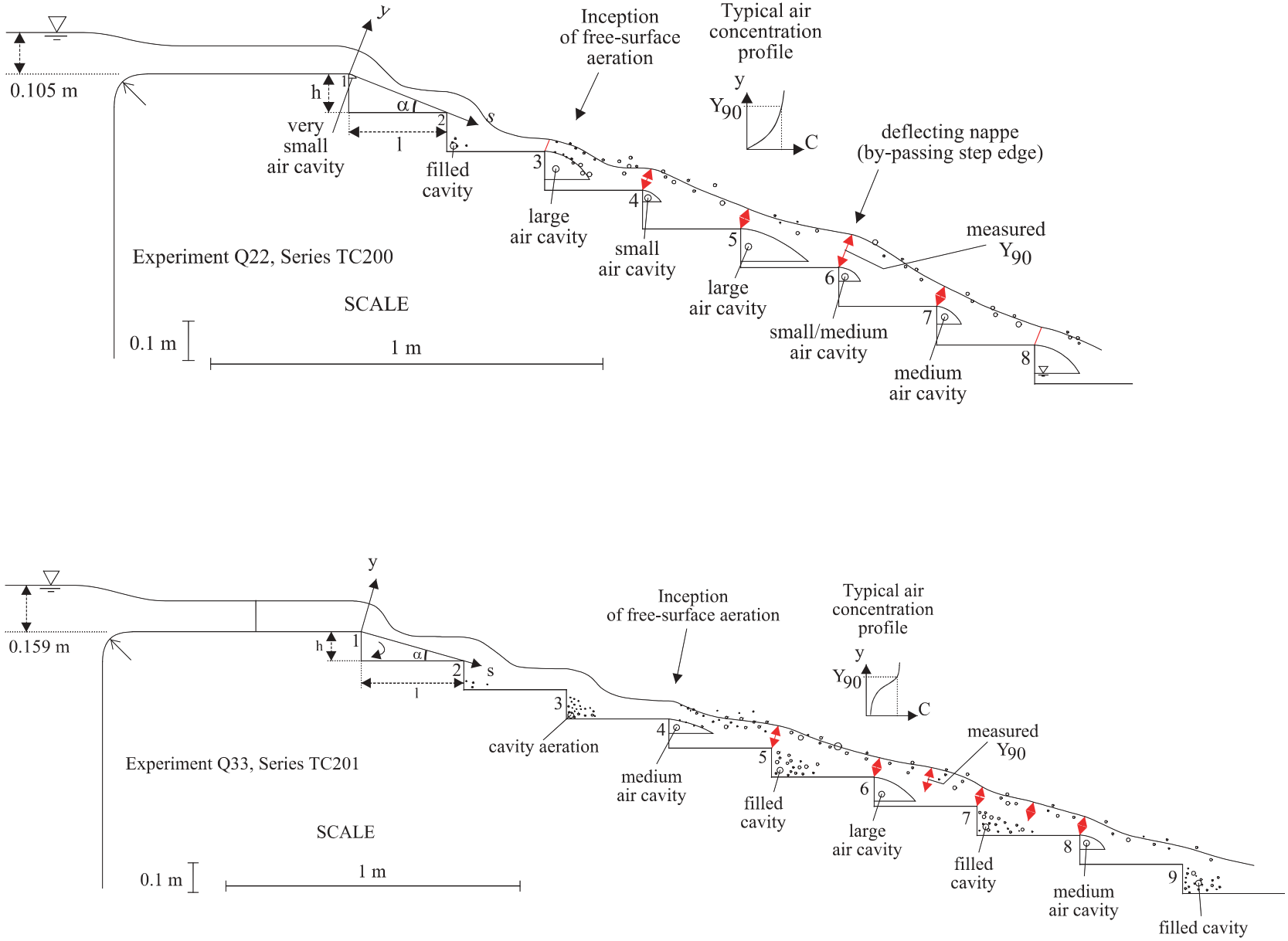

Figure 1 Longitudinal free-surface profiles and air cavities in transition flows (Sketches drawn to scale) Top: sub-regime TRA1, $d_c/h = 0.70$, Run Q22 – Bottom: sub-regime TRA2, $d_c/h = 1.06$, Run Q33.

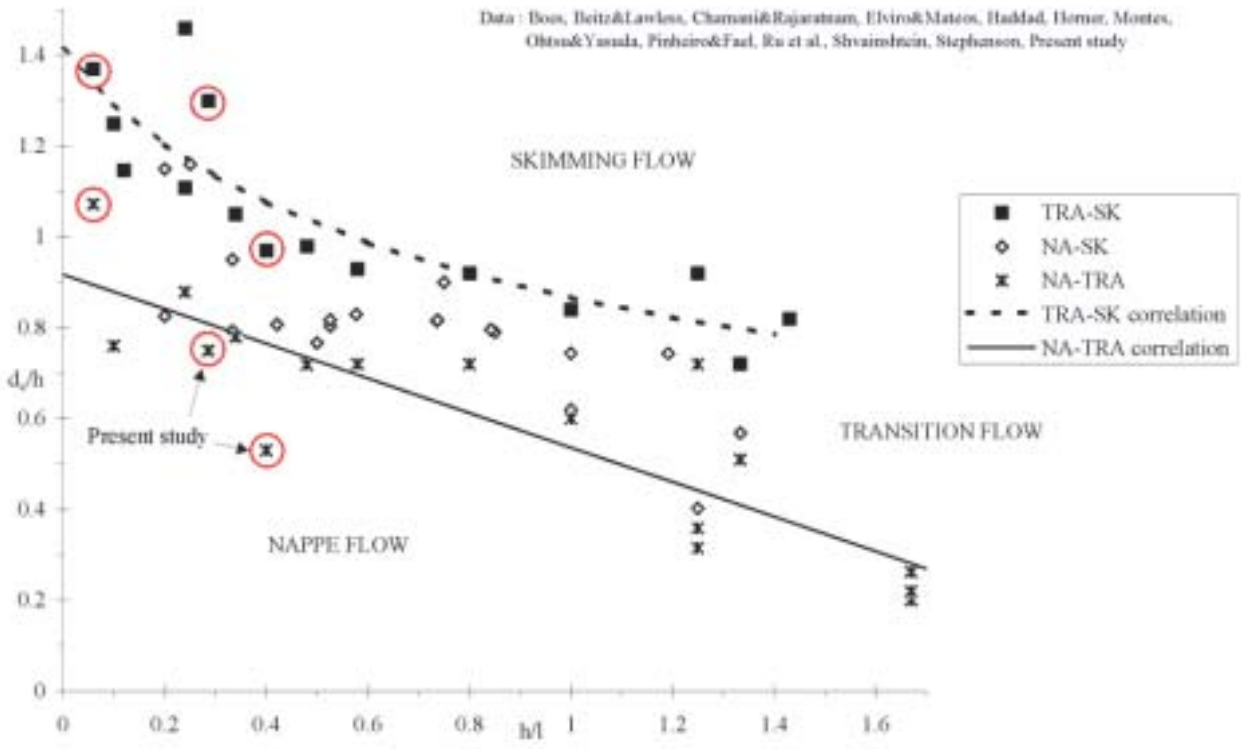

Figure 2 Experimental observations of lower and upper limits of transition flows – Comparison with Eqs. (1) and (2). Experimental data: Beitz And Lawless, Boes, Chamani and Rajaratnam, Elviro and Mateos, Haddad, Horner, Montes, Ohtsu and Yasuda, Pinheiro and Fael, Ru *et al.*, Shvajnshtejn, Stephenson, Present study.

formed by the step edges, and the step cavities were filled at each and every step (i.e. skimming flow regime). For intermediate discharges, the flow exhibited strong splashing and droplet ejections at any position downstream of the inception point of free-surface aeration: i.e. the transition flow regime. For an observer standing on the bank, the transition flow had a chaotic appearance with numerous droplet ejections that were seen to reach heights of up to 3 to 8 times the step height. It did not have the quasi-smooth free-surface appearance of skimming flows, nor the distinctive succession of free-falling nappes observed in nappe flows.

In transition flows down the steep slopes ($\alpha = 16°$ and 22°), the upstream flow was non-aerated. The free-surface exhibited however an undular profile in phase with and of same wave length as the stepped invert profile (Fig. 1). The flow accelerated in the downstream direction until a deflected nappe took place. At take-off, free-surface aeration was observed at both upper and lower nappes with additional air entrainment at the impact followed by jet breakup. Basically the inception of free-surface aeration took place at the first deflected nappe although some bubbles were trapped in cavity(ies) immediately upstream of the nappe take-off. The flow conditions at inception satisfied Fr $\sim$ 4 ($\pm$0.5) for all experiments, where Fr is the flow Froude number at take-off. The observations were very close to both ideal-fluid flow calculations and air-water flow measurements immediately downstream of the inception point. Note that the flow conditions for jet take-off (i.e. Fr $>$ 4) are similar to critical conditions to prevent cavity filling of spillway aeration devices. Chanson (1995a) reviewed the data of Shi *et al.* (1983) and Chanson (1988) yielding Fr $>$ 3 to 6 to avoid cavity drowning and to observe a free jet.

Downstream of the inception point (i.e. first deflected nappe), the flow was highly aerated at each and every step with very significant splashing. The air–water mixture "appears" to flow parallel to the pseudo-bottom formed by the step edges although air cavities existed beneath the nappes. The air cavity shapes alternated from step to step (Fig. 1). Some observations are presented in Fig. 1. Matos (2001) and Ohtsu *et al.* (2001) reported similar observations on stepped spillway models with slopes of 53° and 30 to 55° respectively. Visually, the flow appeared to accelerate above filled cavities and small air cavities, while deceleration occurred at nappe impact immediately downstream of medium to large air cavities. (Air–water flow measurements at step edges confirmed longitudinal fluctuations of the flow velocity around a mean value.)

On the flat slope ($\alpha = 3.4°$), the appearance of the flow was chaotic as in the steep chutes with few differences. The inflow was supercritical (i.e. Fr $>$ 4.5) and a deflected nappe was always observed at the first drop for all experiments. Significant energy dissipation took place immediately downstream of nappe impact and the downstream flow conditions satisfied Fr $\leq$ 4 for all the investigated flows. At each subsequent step, the cavity was filled and contained little air (C $<$ 2%). (This was verified with the conductivity probe). On a horizontal step, dominant flow features were strong spray immediately downstream of nappe impact and the development of shock waves. Downstream of the spray

region, the flow was decelerated until the next brink. (Such a decelerated flow region was not observed on the steeper slopes.)

Experimental results: (2) Upper and lower limits of transition flows

The upper and lower limits of the transition flow regime were recorded. The results are summarised in Table 2 in terms of d_c/h as a function of α, where d_c is the critical depth, h is the step height and α is the slope of the pseudo-bottom formed by the step edges. In the flume 1 (experiments CR98), the lower limit of transition flow was detectable, but no detailed air-water measurements were conducted. In the flumes 2, 3 & 4, the upper and limits were clearly, independently detected by several researchers.

The writers re-analysed previous experimental observations using the same definitions of nappe, transition and skimming flows. The results are plotted in Fig. 2 where the present data are highlighted with a circle. For all the data, the lower and upper limits of transition flows are best correlated by:

$$\frac{d_c}{h} > 0.9174 - 0.381 * \frac{h}{l} \quad \text{Lower limit } (0 < h/1 < 1.7) \qquad (1)$$

$$\frac{d_c}{h} < \frac{0.9821}{(h/l + 0.388)^{0.384}} \quad \text{Upper limit } (0 < h/1 < 1.5) \qquad (2)$$

where l is the step length. Equations (1) and (2) are shown in Fig. 2. The present observations of changes in flow regime are close to the findings of Yasuda and Ohtsu (1999) who found $0.78 < d_c/h < 1.05$ for $\alpha = 18.4°$.

Transition flow sub-regimes

For a given chute geometry, air–water flow measurements (Figs. 3 and 4) suggested two types of transition flows (i.e. sub-regimes). Observed thresholds between each sub-regime are summarised in Table 2 (column 5).

In the lower range of transition flows (sub-regime TRA1), the longitudinal flow pattern was characterised by an irregular alternance of small to large air cavities downstream of the inception point of free-surface aeration (Fig. 1, left). For example, a small air cavity could be observed followed by a larger nappe cavity at the downstream step, then a smaller one. Air concentration measurements showed flat, straight profiles that differ significantly from skimming flow observations (Fig. 3). A deflecting nappe (i.e. by-passing flow) was sometimes observed few steps downstream of the inception point (Fig. 1, left, step edge 6). Liquid fractions (i.e. (1–C)) greater than 10% were measured at distances up to $1.5 * d_c$ while some spray overtopped the 1.25-m high sidewalls. The nappe re-attached the main flow at the next downstream step edge and very large air content was observed: e.g. $C_{mean} = 0.78$ at step edge 6 for $d_c/h = 0.7$ (Fig. 1, left). At the lowest low rates, more than one deflecting flow was sometimes observed: e.g. at step edges 6 and 8 for $d_c/h = 0.6$ ($\alpha = 22°$, run Q16) with $C_{mean} = 0.63$ and 0.68 respectively.

In the upper range of transition flow rates (sub-regime TRA2), the longitudinal flow pattern was characterised by an irregular alternance of air cavities (small to medium) and filled cavities (Fig. 1 Right). The void fraction profiles had a shape similar to skimming flow observations (Fig. 4). A comparison between two free-surface profiles is presented in Fig. 1 based upon two sets of experimental observations.

Experimental results: (3) Air–water flow properties

Air concentration and bubble count rate distributions

In the lower range of flow rates (sub-regime TRA1), air concentration distributions exhibited a straight, flat profile. A set of experimental results is presented in Fig. 3. At most step edges (Fig. 3A and C), the distributions of air concentration may be fitted by an analytical solution of the air bubble advective diffusion equation:

$$C = K''' * \left(1 - \exp\left(-\lambda * \frac{y}{Y_{90}}\right)\right) \quad \text{Sub-regime TRA1} \qquad (3)$$

where y is distance measured normal to the pseudo-invert, Y_{90} is the characteristic distance where $C = 90\%$, and K''' and λ are function of the mean air content only (Appendix). Equation (3) compares favorably with most data, except for the first step edge downstream of the inception point of free-surface aeration and for the deflecting jet flow. Note that Eq. (3) is not valid between step edges (Fig. 3B).

In sub-regime TRA2, air concentration distributions had a smooth, continuous shape (Fig. 4). At step edges, the data follow an analytical solution of the air bubble advective diffusion equation:

$$C = 1 - \tanh^2\left(K'' - \frac{y/Y_{90}}{2 * D_o} + \frac{(y/Y_{90} - 1/3)^3}{3 * D_o}\right) \quad \text{Sub-regime TRA2} \qquad (4)$$

where K'' is an integration constant and D_o is a function of the mean air concentration only (Appendix) (Fig. 4B and 4D). A small number of measurements were taken half-distance between two step edges (e.g. Fig. 4A and 4C). The results suggested consistently a greater overall aeration than at adjacent step edges, and Eq. (4) provided a reasonable estimate of the void fraction profiles. On the flat slope ($\alpha = 3.4°$), a good agreement was observed between data and Eq. (4) along each step, but in the spray region. Overall the results highlight a strong aeration of the flow for all slopes and flow conditions.

Bubble count rate data

Dimensionless distributions of bubble count rates are presented in Figs. 3–5. In Figs. 3 and 4, the data were measured with the double-tip conductivity probe ($\oslash = 25\,\mu m$) while the data in Fig. 5 were recorded with the single-tip probe ($\oslash = 300\,\mu m$). (The bubble count rate data are function of the probe sensor size. Bubble count rates measured with the double-tip probe were about twice those detected by the single-tip probe at the same location with identical flow conditions.)

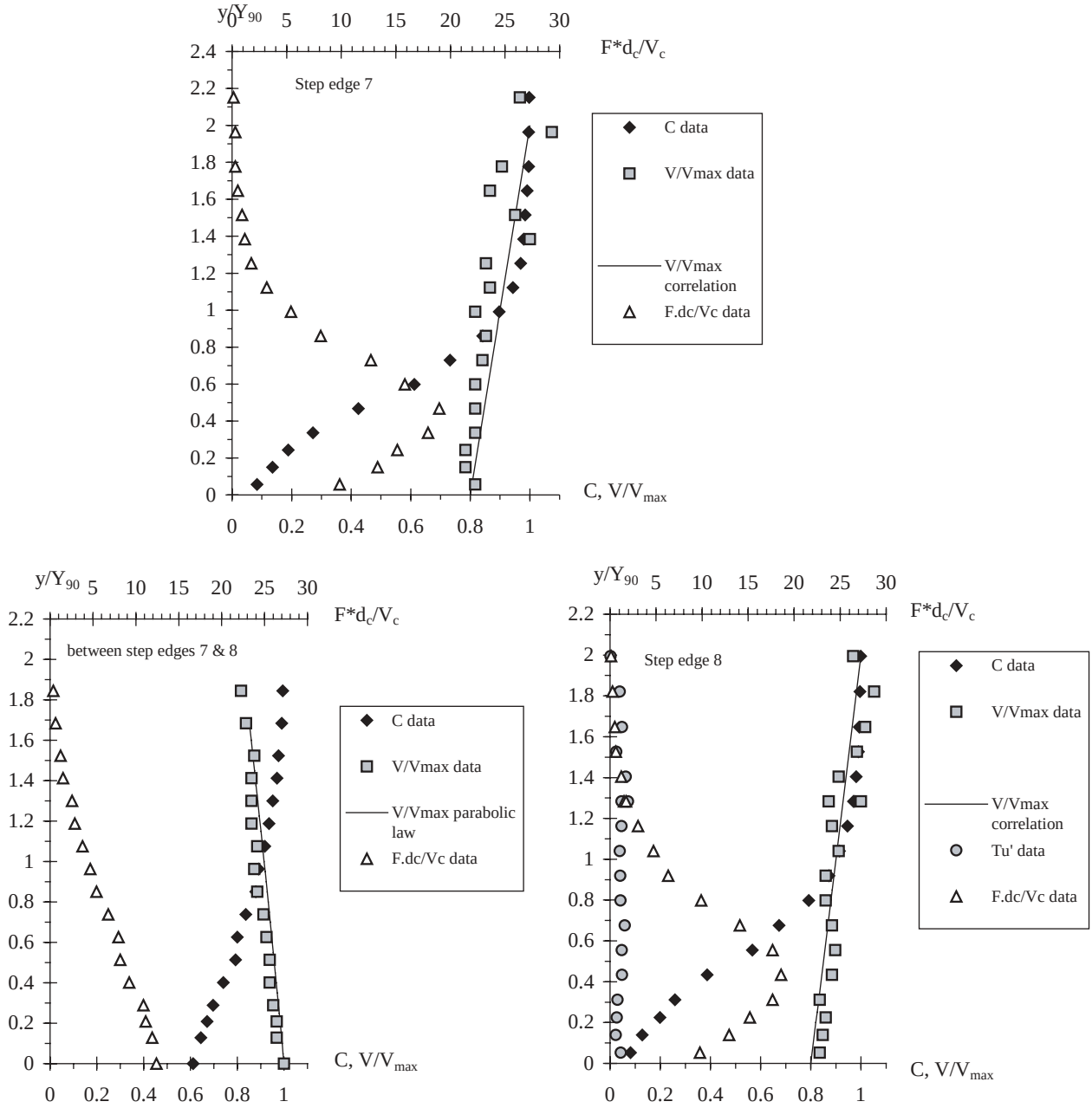

Figure 3 Air–water flow properties in transition flow, sub-regime TRA1 ($d_c/h = 0.78$, $rmh = 0.1$ m, $\alpha = 15.9°$, inception point at the 3rd step edge) – Comparison between data and Eqs. (3), (8) and (10).

Figure	3A	3B	3C
Y_{90} (m)	0.0535	0.0623	0.0577
V_{max} (m/s)	2.68	2.51	2.55
Location	at step edge	1/2 distance between step edges (medium air cavity)	at step edge

Overall the data followed approximately a parabolic law:

$$\frac{F}{F_{max}} = 4 * C * (1 - C) \quad (5)$$

where F_{max} is the maximum bubble count rate observed for $C = 50\%$. Data are compared with Eq. (5) in Fig. 5. Toombes (2002) demonstrated the unicity of the relationship between bubble frequency and void fraction, although he proposed a more sophisticated model comparing favorably with experimental data obtained in water jets discharging into air, smooth-chute flows and stepped chute flows.

Discussion

Equations (3) and (4) are analytical solutions of the advective diffusion of air bubbles. They were developed assuming the following distributions of dimensionless turbulent diffusivity of air

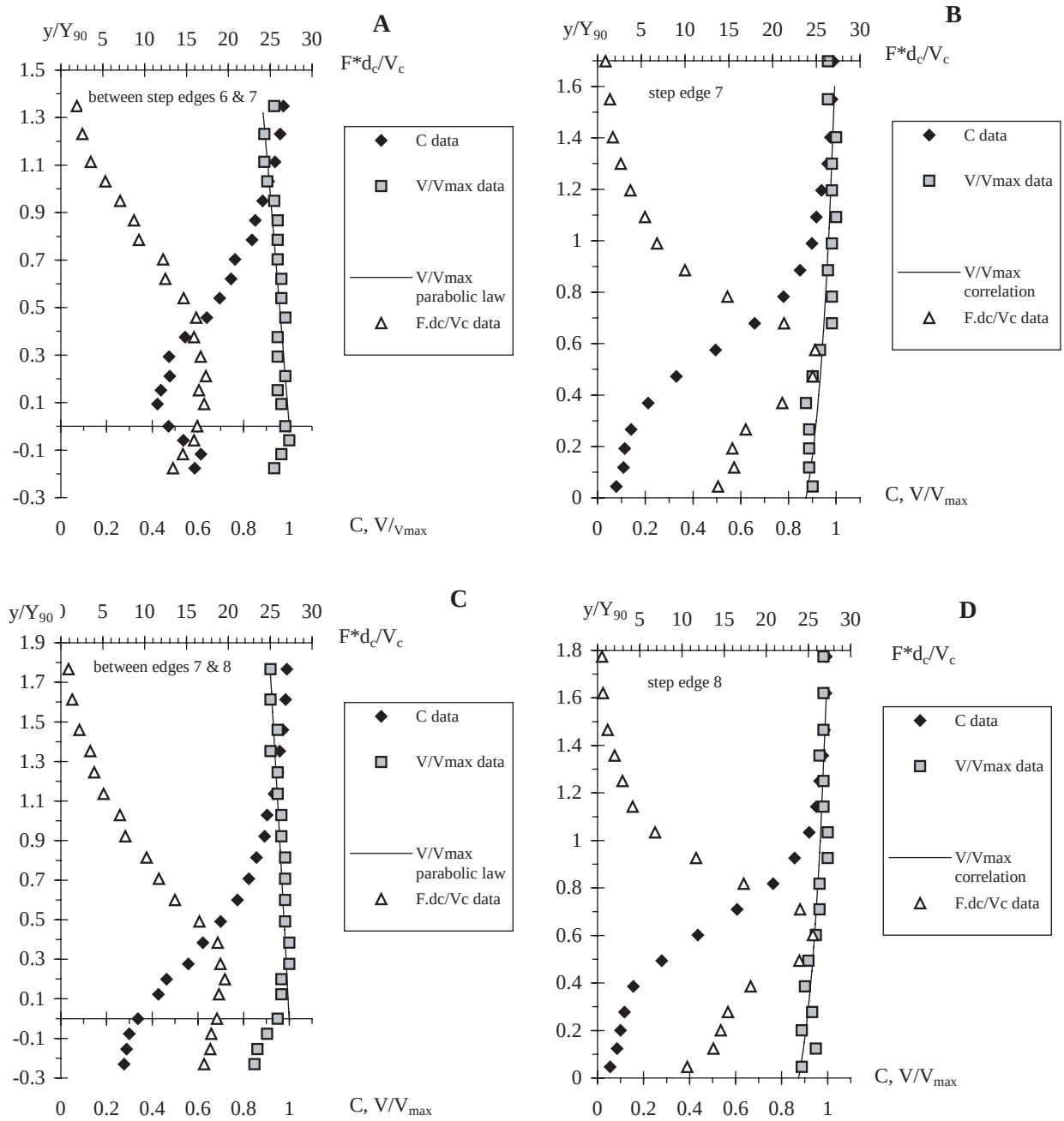

Figure 4 Air–water flow properties in transition flow, sub-regime TRA2 ($d_c/h = 1.06$, $h = 0.1$ m, $\alpha = 15.9°$, inception point at the 4th step edge) – Comparison between data and Eqs. (4), (9) and (10).

Figure	4A	4B	4C	4D
Y_{90} (m)	0.0853	0.0677	0.0651	0.0648
V_{max} (m/s)	2.73	2.83	2.78	2.83
Location	1/2 distance between step edges (large air cavity)	at step edge	1/2 distance between step edges (filled cavity)	at step edge

bubbles:

$$D' = \frac{C * \sqrt{1-C}}{\lambda * (K''' - C)} \quad \text{Sub-regime TRA1} \tag{6}$$

$$D' = \frac{D_o}{1 - 2 * (y/Y_{90} - 1/3)^2} \quad \text{Sub-regime TRA2} \tag{7}$$

where $D' = D_t/((u_r)_{Hyd} * \cos\alpha * Y_{90})$, D_t is the turbulent diffusivity, $(u_r)_{Hyd}$ is the rise velocity in hydrostatic pressure gradient (Appendix). Note that the shape of Eq. (6) is similar to the sediment diffusivity distribution developed by Rouse (1937) which yields to the Rouse distribution of suspended matter (e.g. Nielsen, 1992; Chanson, 1999).

Velocity distributions

Air–water velocity measurements showed flat, straight velocity profiles at step edges for all flow conditions and for $y/Y_{90} < 2$

Table 2 Lower and upper limits of the transition flow regime.

Experiments	Slope α(°)	h (m)	d_c/h			Remarks
			NA-TRA	TRA1-TRA2	TRA-SK	
(1)	(2)	(3)	(4)	(5)	(6)	(7)
Flume 1	3.4	0.143	1.07	–	–	Experiments CR98.
Flume 2	3.4	0.0715	1.07	(<1.2)	1.37	Experiments EV200a.
Flume 3	15.9	0.10	0.75	0.93	1.30	Experiments TC201.
Flume 4	21.8	0.10	0.53	0.75	0.97	Experiments TC200 & EV200b.

Notes: NA-TRA = lower limit of transition flow; TRA1-TRA2 = onset of sub-regime TRA2; TRA-SK = upper limit of transition flow.

(A) Flume 2 : α = 3.4º, h = 0.071 m, d_c/h = 1.22, step 16

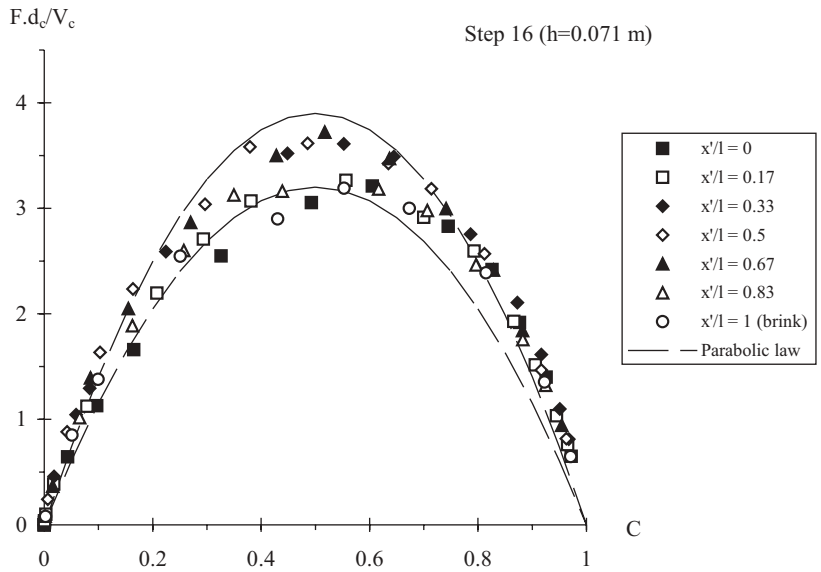

(B) Flume 3 : α = 21.8º, h = 0.10 m, d_c/h = 0.75, inception at 3rd step edge

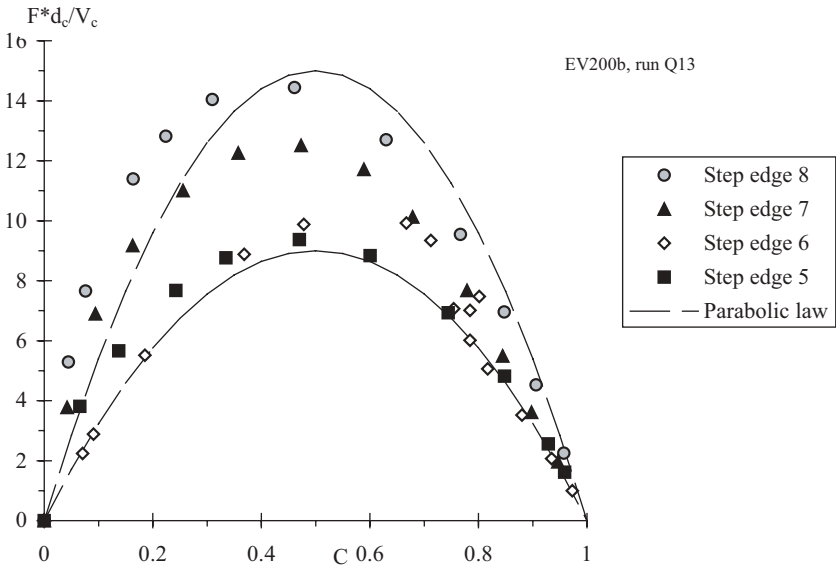

Figure 5 Dimensionless distributions of bubble count rates – Comparison with Eq. (5).

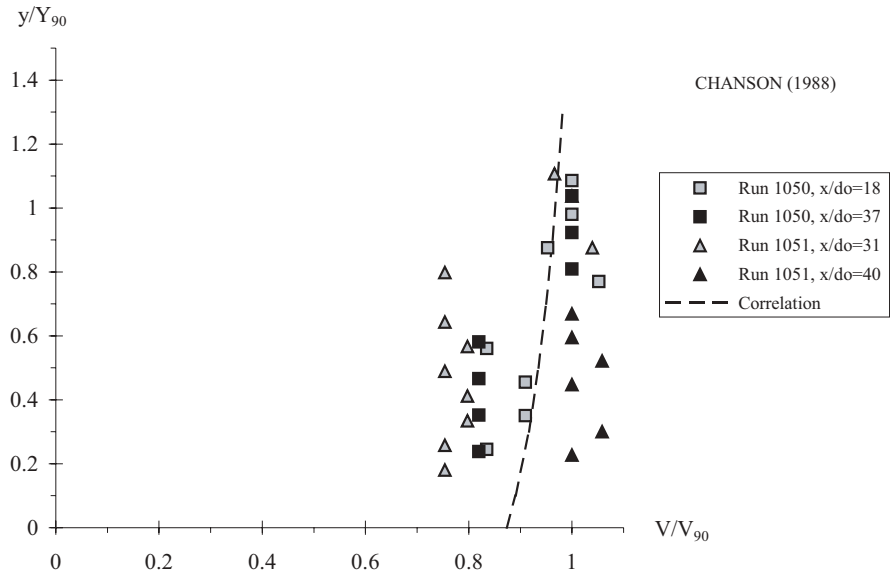

Figure 6 Dimensionless velocity distributions in the impact region downstream of a spillway aeration device (Data: Chanson, 1988) – Comparison between data and Eq. (9).

(Figs. 3 and 4). It is believed that large energy dissipation at each step is associated with very-energetic turbulent mixing across the entire air–water flow. In turn the strong momentum mixing yields quasi-uniform velocity profiles. Overall the data at step edges were correlated by:

$$\frac{V}{V_{max}} \sim 0.8 + 0.1 * \left(\frac{y}{Y_{90}}\right)$$
sub-regime TRA1 ($y/Y_{90} < 2$) (8)

$$\frac{V}{V_{max}} \sim 0.95 * \left(\frac{y}{Y_{90}} + 0.3\right)^{0.07}$$
sub-regime TRA2 ($y/Y_{90} < 1.6$) (9)

Equations (8) and (9) are shown in Figs. 3A and C, and 4B and D respectively. They are very-rough estimate without theoretical background. The velocity results differ significantly from skimming flow data: e.g. Matos (2000) and Chanson and Toombes (2001) observed a 1/5 to 1/6-th power law at step edges.

Velocity data in transition flows are somehow similar to (1) detailed air-water measurements immediately downstream of nappe impact in nappe flows (Toombes, 2002) and to (2) air–water data in the impact region of spillway aeration device flows (Chanson, 1988). Figure 6 compares the latter set of data with Eq. (9). Despite some scatter associated with the crude instrumentation, some agreement is seen.

At half-distance between step edges (Figs. 3B and 4A and C), the velocity distributions showed a marked change from observations at step edges. The data were similar to ideal-fluid flow velocity profiles in free-falling jet downstream of an overfall. Extending the reasoning of Montes (1998, p. 216), the velocity distribution in the jet may be analytically derived as:

$$\frac{V}{V_{90}} = \sqrt{1 - 2 * \frac{y/Y_{90}}{Fr^2}}$$
between step edges (for $y/Y_{90} > 0$) (10)

where Fr is the inflow Froude number at the upstream step edge. Equation (10) assumes an uniform velocity profile upstream of jet take-off and neglects the effect of an upstream boundary layer. Figures 3B and 4A and C shows a close agreement between Eq. (10) and the data (sub-regimes TRA1 and TRA2), including above a filled cavity (Fig. 4C).

Discussion

A characteristic feature of transition flow was the intense splashing and strong free-surface aeration which was observed on all slopes for all experiments. Figure 7 presents depth-averaged data showing the mean air concentration C_{mean} as a function of the dimensionless distance x/d_c from the upstream end of the chute. (Note the logarithmic scale of the horizontal axis.) Figure 7 includes data measured at step edges and between step edges. The results show mean air contents larger then acknowledged mean air concentrations in smooth-invert and skimming flows. For example, the re-analysis of Straub and Anderson's (1958) data on smooth-inverts yields maximum (equilibrium) mean air concentration of 0.07, 0.25 and 0.30 for $\alpha = 3.4°$, 16° and 22° respectively. Observed air contents in transition flows were about twice to three times larger (Fig. 7).

The flow resistance was estimated based upon air-water flow properties measured at step edges. The Darcy friction factor was calculated as

$$f_e = \frac{8 * g}{q_w^2} * \left(\int_{y=0}^{y=Y_{90}} (1 - C) * dy\right)^3 * S_f \quad (11)$$

where f_e is the Darcy friction factor for air–water flow, g is the gravity acceleration, q_w is the water discharge per unit width, S_f is the friction slope ($S_s = -\partial H/\partial x$), H is the total head and x is the distance in the flow direction. The results based upon total head data calculated at step edges are summarised in Table 3 and they are compared with flow resistance observations in nappe flows

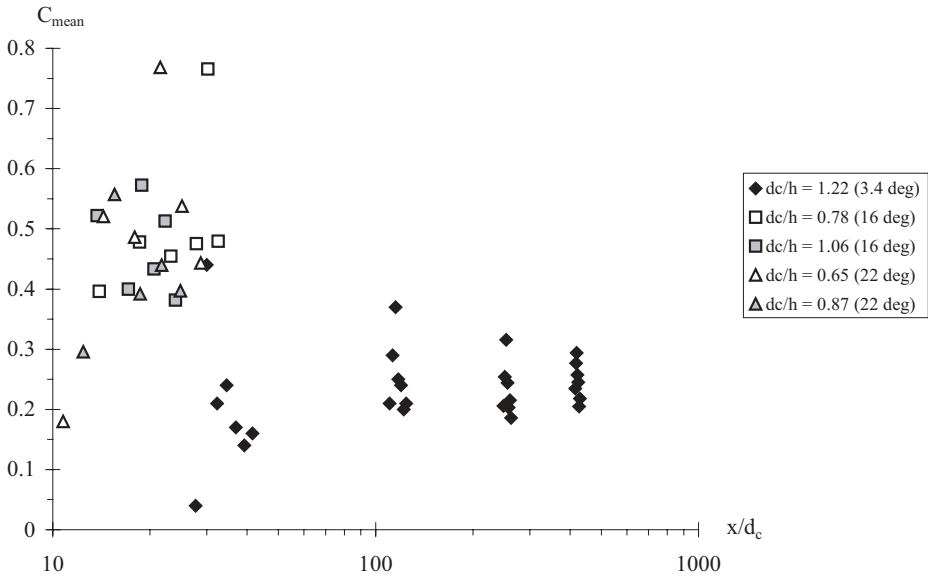

Figure 7 Longitudinal variations of the mean air concentration.

Table 3 Flow resistance estimates based upon detailed air–water flow measurements.

Ref. (1)	Flow regime (2)	d_c/h (3)	f_e (4)	Remarks (5)
Flume 1	Nappe flow	0.6–0.95	0.07–0.096	Single tip probe data. Experiments CR_98.
Flume 2	Transition flow	1.22	0.029	Single-tip probe data. Experiments EV200a.
	Skimming flow	1.5–1.9	0.034–0.042	
Flume 3	Transition flow	0.6–1.0	0.125–0.244	Single-tip and double-tip probe data. Experiments TC200 & EV200b.
	Skimming flow	1.05–1.5	0.074–0.283	
Flume 4	Transition flow	0.78–1.06	0.105–0.107	Double-tip probe data. Experiments TC201.
	Skimming flow	1.54	0.14	

and skimming flows in the same facilities. Overall, the friction factor data in transition flows are comparable to flow resistance data in skimming and nappe flows in the same facilities. For $3.4 \leq \alpha \leq 22°$, the flow resistance tends to increase with the bed slope as observed by Ohtsu and Yasuda (1997) in skimming flows.

The strong flow aeration and relatively-slow flow velocity (compared to smooth chutes) yield large air–water interfacial area and large residence times. Both contribute strong air–water mass transfer, and it is suggested that the transition flows might be a suitable flow regime to maximise air–water gas transfer down a stepped cascade.

Conclusion

The present study demonstrates the existence of a transitory flow regime for intermediate flow rates between nappe and skimming flows. The transition flow regime does not have the quasi-smooth free-surface appearance of skimming flows, nor the distinctive succession of free-falling nappes observed in nappe flows. It is characterised by a chaotic behaviour associated with intense splashing and strong free-surface aeration.

The lower and upper limits of transition flows are presented in Table 2 and Fig. 2. Detailed air–water flow measurements highlight two sub-regimes. For low flow rates, the longitudinal flow pattern is characterised by irregular succession of small and large air cavities at each step, associated with almost linear air concentration distributions (Fig. 3). For larger flow rates, some cavities are filled and the air concentration distributions have the same shape as in skimming flows (Fig. 4).

Air–water velocity measurements showed nearly straight distributions at step edges. It is proposed that strong turbulent mixing across the flow contributes to quasi-uniform velocity profiles. Between step edges, the velocity distributions may be predicted by ideal-fluid calculations for free-falling nappes.

In summary the transition flows have very different characteristics from both nappe and skimming flows. Dominant features include intense droplet ejection and spray. Measured air contents were two to three times larger than those recorded in smooth chutes and skimming flows, and the strong aeration might be suitable to enhance air–water gas transfer.

Acknowledgments

The authors acknowledge the assistance of M. Eastman, N. Van Schagen. The first writer thanks Dr Y. Yasuda and Professor I. Ohtsu for their helpful comments.

Appendix: Air bubble diffusion in transition flows

Free-surface aeration occurs when turbulence acting next to the free-surface is large enough to overcome both surface tension for the entrainment of air bubbles and buoyancy to carry downwards the bubbles. At uniform equilibrium, the air concentration distribution is a constant with respect to the distance x in the flow direction. The continuity equation for air in the air-water flow yields:

$$\frac{\partial}{\partial y}\left(D_t * \frac{\partial C}{\partial y}\right) = \cos\alpha * \frac{\partial}{\partial y}(u_r * C) \quad (A.1)$$

where D_t is the air bubble turbulent diffusivity, u_r is the bubble rise velocity, α is the channel slope and y is measured perpendicular to the mean flow direction. The bubble rise velocity in a fluid of density $\rho_w * (1-C)$ equals: $u_r = (u_r)_{Hyd} * \sqrt{1-C}$ where $(u_r)_{Hyd}$ is the rise velocity in hydrostatic pressure gradient (Chanson, 1995b). A first integration of the continuity equation for air in the equilibrium flow region leads to:

$$\frac{\partial C}{\partial y'} = \frac{1}{D'} * C * \sqrt{1-C} \quad (A.2)$$

where $y' = y/Y_{90}$ and $D' = D_t/((u_r)_{Hyd} * \cos\alpha * Y_{90})$ is a dimensionless turbulent diffusivity.

Chanson (1995b) solved Eq. (A.2) assuming a homogeneous turbulence across the flow (i.e. D' constant). Chanson and Toombes (2001) detailed further analytical models of void fraction distributions assuming a non constant diffusivity D'. Results were successfully compared with transition and skimming air–water flow data. Toda and Inoue (1997) developed two-dimensional numerical models of the advective diffusion equation for air bubbles. The results of both Lagrangian and Eulerian models gave very similar results to air-water flow measurements and to the analytical models of Chanson and Toombes (2001).

Notations

C = air concentration defined as the volume of air per unit volume, also called void fraction
C_{mean} = depth averaged air concentration defined as: $C_{mean} = \frac{1}{Y_{90}} * \int_{y=0}^{Y_{90}} C * dy$
D_t = turbulent diffusivity (m^2/s) of air bubble in air–water flows
D_o = dimensionless coefficient
D' = dimensionless air bubble diffusivity (defined by Chanson, 1995b)
d_c = critical flow depth (m); for a rectangular channel: $d_c = \sqrt[3]{q_w^2/g}$
d_o = inflow depth (m)
F = bubble count rate (Hz): i.e. number of bubbles detected by the probe sensor per second
F_{max} = maximum bubble count rate (Hz)
Fr = Froude number
f_e = Darcy friction factor of air–water flows
g = gravity constant (m/s^2); g = 9.80 m/s^2 in Brisbane
H = total head (m)
h = height of steps (m) (measured vertically)
K', K'', K''' = integration constants
L = chute length (m)
l = horizontal length of steps (m) (measured perpendicular to the vertical direction)
q_w = water discharge per meter width (m^2/s)
S_f = friction slope
u_r = bubble rise velocity (m/s)
$(u_r)_{Hyd}$ = bubble rise velocity (m/s) in a hydrostatic pressure gradient
V = air–water velocity (m/s)
V_c = critical velocity (m/s); for a rectangular channel: $V_c = \sqrt[3]{g * q_w}$
V_{max} = maximum velocity (m/s)
W = chute width (m)
x = longitudinal distance (m)
x' = horizontal distance (m) measured from the vertical step face
y = 1 – distance (m) from the bottom measured perpendicular to the spillway invert
= 2 – distance (m) from the pseudo-bottom (formed by the step edges) measured perpendicular to the flow direction

Greek symbols

α = channel slope
λ = dimensionless coefficient
$\oslash$ = diameter (m)

Subscript

c = critical flow conditions

References

1. BACARA (1991). "Etude de la Dissipation d'Energie sur les Evacuateurs à Marches." ('Study of the Energy Dissipation on Stepped Spillways.') *Rapport d'Essais*, Projet National BaCaRa, CEMAGREF-SCP, Aix-en-Provence, France, Oct., 111 pages (in French).
2. BEITZ, E. and LAWLESS, M. (1992). "Hydraulic Model Study for dam on GHFL 3791 Isaac River at Burton Gorge," *Water Res. Commission Report*, Ref. No. REP/24.1, Sept., Brisbane, Australia.
3. BOES, R.M. (2000). "Zweiphasenstroömung und Energieumsetzung an Grosskaskaden." ('Two-Phase Flow and Energy Dissipation on Cascades.') *PhD thesis*, VAW-ETH, Zürich, Switzerland (in German). (also *Mitteilungen der Versuchsanstalt fur Wasserbau, Hydrologie und Glaziologie*, ETH-Zurich, Switzerland, No. 166).
4. BOS, M.G. (1976). "Discharge Measurement Structures," *Publication No. 161*, Delft Hydraulic Laboratory, Delft, The

Netherlands (also Publication No. 20, ILRI, Wageningen, The Netherlands).
5. CHAMANI, M.R. and RAJARATNAM, N. (1999). "Onset of Skimming Flow on Stepped Spillways," *J. Hydr. Engrg.* ASCE, 125(9), 969-971. Discussion: 127(6), 519–525.
6. CHANSON, H. (1988). "A Study of Air Entrainment and Aeration Devices on a Spillway Model," *PhD thesis*, Ref. 88-8, Dept. of Civil Engrg., University of Canterbury, New Zealand (ISSN 0110-3326).
7. CHANSON, H. (1995a). "Predicting the Filling of Ventilated Cavities behind Spillway Aerators," *J. Hydr. Res.* IAHR, 33(3), 361–372.
8. CHANSON, H. (1995b). "Air Bubble Diffusion in Supercritical Open Channel Flow," *Proc. 12th Australasian Fluid Mechanics Conference AFMC*, Sydney, Australia, R.W. BILGER Ed., Vol. 2, pp. 707–710 (ISBN 0 86934 034 4).
9. CHANSON, H. (1996). "Prediction of the Transition Nappe/Skimming Flow on a Stepped Channel," *J. Hydr. Res.* IAHR, 34(3), 421–429 (ISSN 0022-1686).
10. CHANSON, H. (1999). "The Hydraulics of Open Channel Flows: An Introduction," Butterworth-Heinemann, Oxford, UK, 512 pages.
11. CHANSON, H. and TOOMBES, L. (1998). "Supercritical Flow at an Abrupt Drop: Flow Patterns and Aeration," *Can. J. Civil Engrg.*, 25(5), 956–966.
12. CHANSON, H. and TOOMBES, L. (2001). "Experimental Investigations of Air Entrainment in Transition and Skimming Flows down a Stepped Chute. Application to Embankment Overflow Stepped Spillways," *Research Report No. CE158*, Dept. of Civil Engrg., University of Queensland, Brisbane, Australia, July.
13. CHANSON, H., YASUDA, Y. and OHTSU, I. (2000). "Flow Resistance in Skimming Flow: A Critical Review," *Int. Workshop on Hydraulics of Stepped Spillways*, Zürich, Switzerland, H.E. Minor and W.H. Hager Eds., Balkema Publ., pp. 95–102 (ISBN 90 5809 135X).
14. ELVIRO, V. and MATEOS, C. (1995). "Spanish Research into Stepped Spillways," *Int. J. Hydropower & Dams*, 2(5), 61–65.
15. HADDAD, A.A. (1998). "Water Flow Over Stepped Spillway," *Masters Thesis*, Polytechnic of Bari, Italy.
16. HENDERSON, F.M. (1966). "Open Channel Flow," MacMillan Company, New York, USA.
17. HORNER, M.W. (1969). "An Analysis of Flow on Cascades of Steps," *PhD thesis*, Univ. of Birmingham, UK, May, 357 pages.
18. MATOS, J. (2000). "Hydraulic Design of Stepped Spillways over RCC Dams," *Int. Workshop on Hydraulics of Stepped Spillways*, Zürich, Switzerland, H.E. Minor and W.H. Hager Eds., Balkema Publ., pp. 187–194.
19. MATOS, J. (2001). "Onset of Skimming Flow on Stepped Spillways. Discussion," *J. Hydr. Engrg.* ASCE, 127(6), 519–521.
20. MONTES, J.S. (1994). Private Communication.
21. MONTES, J.S. (1998). Hydraulics of Open Channel Flow. ASCE Press, New York, USA, 697 pages.
22. NIELSEN, P. (1992). "Coastal Bottom Boundary Layers and Sediment Transport," *Advanced Series on Ocean Engrg.*, Vol. 4, World Scientific Publ., Singapore.
23. OHTSU, I. and YASUDA, Y. (1997). "Characteristics of Flow Conditions on Stepped Channels," *Proc. 27th IAHR Biennal Congress*, San Francisco, USA, Theme D, pp. 583–588.
24. OHTSU, I., YASUDA, Y. and TAKAHASHI, M. (2001). "Onset of Skimming Flow on Stepped Spillways. Discussion," *J. Hydr. Engrg.* ASCE, 127(6), 522–524.
25. PINHEIRO, A.N. and FAEL, C.S. (2000). "Nappe Flow in Stepped Channels – Occurrence and Energy Dissipation," *Int. Workshop on Hydraulics of Stepped Spillways*, Zürich, Switzerland, H.E. Minor and W.H. Hager Eds,, Balkema Publ., pp. 119–126.
26. RAJARATNAM, N. (1990). "Skimming Flow in Stepped Spillways," *J. Hydr. Engrg.* ASCE, 116(4), 587–591. Discussion: 118(1), 111–114.
27. ROUSE, H. (1937). "Modern Conceptions of the Mechanics of Turbulence," *Transactions* ASCE, 102, 463–543.
28. RU, S.X., TANG, C.Y., PAN, R.W. and HE, X.M. (1994). "Stepped Dissipator on Spillway Face," *Proc. 9th APD-IAHR Congress*, Singapore, Vol. 2, pp. 193–200.
29. SHI, Q., PAN, S., SHAO, Y. and YUAN, X. (1983). "Experimental Investigation of Flow Aeration to prevent Cavitation Erosion by a Deflector," *Shuili Xuebao* (*J. Hydr. Engrg.*), Beijing, China, 3, 1–13 (in Chinese).
30. SHVAJNSHTEJN, A.M. (1999). "Stepped Spillways and Energy Dissipation," *Gidrotekhnicheskoe Stroitel'stvo*, No. 5, pp. 15–21 (in Russian). (Also *Hydrotechnical Construction*, 3(5), 1999, 275–282.)
31. STEPHENSON, D. (1979). "Gabion Energy Dissipators," *Proc. 13th ICOLD Congress*, New Delhi, India, Q. 50, R. 3, pp. 33–43.
32. STRAUB, L.G. and ANDERSON, A.G. (1958). "Experiments on Self-Aerated Flow in Open Channels," *J. Hydr. Div.* Proc. ASCE, 84(HY7), 1890-1–1890-35.
33. TODA, K. and INOUE, K. (1997). "Advection and Diffusion properties of Air Bubbles in Open Channel Flow," *Proc. 27th IAHR Congress*, San Francisco, USA, Theme B, F.M. Holly Jr. and A. Alsaffar Ed., Vol. 1, pp. 76–81.
34. TOOMBES, L. (2002). "Experimental Study of Air–Water Flow Properties on low-gradient Stepped Cascades," Ph.D. thesis, Dept of Civil Engrg., University of Queensland, Brisbane, Australia.
35. YASUDA, Y. and OHTSU, I.O. (1999). "Flow Resistance of Skimming Flow in Stepped Channels," *Proc. 28th IAHR Congress*, Graz, Austria, Session B14, 6 pages.